Photoexcited Muon Spin Spectroscopy: A New Method for Measuring Excess Carrier Lifetime in Bulk Silicon

K. Yokoyama,[1,2,*] J. S. Lord,[2] J. Miao,[1,3] P. Murahari,[1] and A. J. Drew[1,2,3,†]
[1]School of Physics and Astronomy, Queen Mary University of London, Mile End, London E1 4NS, United Kingdom
[2]ISIS, STFC Rutherford Appleton Laboratory, Didcot OX11 0QX, United Kingdom
[3]College of Physical Science and Technology, Sichuan University, Chengdu 610064, People's Republic of China
(Received 27 February 2017; revised manuscript received 7 November 2017; published 29 November 2017)

We have measured excess carrier lifetime in silicon using photoexcited muon spin spectroscopy. Positive muons implanted deep in a wafer can interact with the optically injected excess carriers and directly probe the bulk carrier lifetime while minimizing the effect from surface recombination. The method is based on the relaxation rate of muon spin asymmetry, which depends on the excess carrier density. The underlying microscopic mechanism has been understood by simulating the four-state muonium model in Si under illumination. We apply the technique to different injection levels and temperatures, and demonstrate its ability for injection- and temperature-dependent lifetime spectroscopy.

DOI: 10.1103/PhysRevLett.119.226601

Excess carrier lifetime in semiconductors is an extremely sensitive probe of recombination active defect density N_t [1,2]. In the case of silicon, a lifetime spectroscopy can probe N_t as low as 10^{10} cm^{-3}, corresponding to the carrier lifetime in the order of 10 ms. Therefore the lifetime measurements have been utilized to test a quality of Si wafers in various areas, and especially appreciated in photovoltaic applications where the carrier lifetime is a key parameter for the excess carriers to successfully diffuse across the p-n junction in solar cells. The microchip industries have also found its use as a cleanliness monitor in the chip manufacturing processes. It is now widely accepted that there are three main mechanisms that cause the electron-hole pair (EHP) recombination in semiconductors: (1) Shockley-Read-Hall (SRH) recombination (characterized by its lifetime τ_{SRH}), (2) Auger recombination (τ_{Auger}), and (3) radiative recombination (τ_{rad}) [1,2]. The bulk recombination lifetime τ_{bulk} is then given by a relation, $\tau_{\mathrm{bulk}}^{-1} = \tau_{\mathrm{SRH}}^{-1} + \tau_{\mathrm{Auger}}^{-1} + \tau_{\mathrm{rad}}^{-1}$. Among those mechanisms, the SRH recombination is a multiphonon process mediated by deep-level defect centers, and dominates τ_{bulk} in low-level carrier injections, while the Auger recombination plays a key role in high-level injections. The radiative recombination is usually negligible in bulk Si due to the indirect band structure.

Although τ_{SRH} gives a good indication of the N_t level, it alone cannot determine N_t explicitly—it is always necessary to assume the defect type, which is characterized by its energy level and capture cross section for electrons and holes. Deep level transient spectroscopy (DLTS) is commonly utilized to investigate the defect centers [1–3]. However Rein *et al.* [2,4] proposed that injection- and temperature-dependent lifetime spectroscopy (IDLS and TDLS) could provide a direct identification of the defect types. The techniques have been demonstrated for Si samples with intentionally introduced metal impurities [4,5].

To measure the carrier lifetime, there are a few traditional methods, such as the photoconductance decay (PCD) and photoluminescence decay measurements. Induction-coupled PCD is becoming more popular by virtue of their contactless and nondestructive measurement [1,2,6]. These techniques measure, by their nature, the effective lifetime of injected carriers, given by $\tau_{\mathrm{eff}}^{-1} = \tau_{\mathrm{bulk}}^{-1} + \tau_S^{-1}$. The second term represents a contribution from the surface lifetime τ_S that strongly depends on how the wafer surface has been conditioned. It is therefore necessary to extract τ_{bulk} by (1) treating the surface to make τ_S asymptote either 0 (e.g., sandblasting) or ∞ (e.g., passivation), or (2) measuring the same samples with different thicknesses d and extrapolating the observed lifetimes for $1/d \to 0$. Although these methods are established and widely used, there are few experimental techniques to directly measure τ_{bulk}, minimizing uncertainties associated with the surface recombination. Those techniques can be important not only in the semiconductor engineering but also in the fundamental understanding of the EHP kinetics.

In this Letter we demonstrate a use of positively charged (anti)muon μ^+ as a contactless probe of τ_{bulk} in Si. Spin-polarized μ^+ with an energy of 4 MeV ("surface" muons) are generated in a proton accelerator facility and implanted in bulk materials with the distribution thermalizing over several hundred μm. In a case of Si, the implantation depth can be as deep as 700 μm, where the surface effect is negligibly small in most cases. Our recent upgrade of the HiFi muon spectrometer at the ISIS pulsed neutron and muon source in the UK enables us to photoexcite samples with a high-energy laser pulse [7–9]. A pulsed muon source is useful for time-differential studies, as well as for achieving a large stimulation by virtue of the high-intensity

light source. The sample temperature can be controlled using cryostats and hot stages available in the HiFi experimental suite [7,10]. Combining these capabilities, muon spin spectroscopy (μSR) can not only measure the excess carrier lifetime but also investigate its injection and temperature dependence. The muons are an extremely dilute impurity ($<10^5$ cm^{-3}) and although the muon centers cause recombination, they should have a negligible effect on the carrier lifetime compared to the other impurities present.

Upon implantation, muons decay with a lifetime of 2.2 μs and emit positrons preferentially in the muon spin direction, which is then subsequently detected. The obtained time spectrum for muon spin asymmetry carries information on the muon state and its interaction with local atomic and/or electronic environment [11,12]. The μSR technique has been applied to many semiconductor systems, especially to single crystal Si [13,14]. There have been several μSR studies on illuminated Si, which report a large photoinduced change in the μSR time spectrum [15–18].

In semiconductors, an implanted μ^+ can capture an electron to form a muonium atom ($\mathrm{Mu} = \mu^+ + e^-$), a radioisotope of hydrogen. As with H, Mu can exist in three charge states in semiconductors: Mu^0, Mu^+, and Mu^-. In addition, in the case of Si, there are two distinct lattice sites for Mu to occupy: the bond-center site (Mu_{BC}) and the interstitial tetrahedral site (Mu_T). The charge state and lattice site depend on the formation energy determined by the dopant type, concentration, and temperature. For instance, the initial muon asymmetry in intrinsic Si in room temperature (RT) consists of nearly equal amount of Mu^+_{BC} and Mu^0_T component. The diamagnetic Mu^+_{BC} fraction decreases monotonically as the temperature decreases from 250 K down to 200 K. This behavior is attributed to slowing down of the thermally activated ionization of Mu^0_{BC} into Mu^+_{BC} centers. Therefore, almost the same amount of Mu^0_{BC} and Mu^0_T can be found in low temperatures, such as $T = 77$ K [13,14]. Upon illumination, injected excess carriers start interacting with the Mu centers in a complex mechanism, including spin exchange interaction, cyclic charge exchange reaction, and site change reaction [7,14–18]. These interactions result in a spin relaxation of the bound electron in Mu, which then depolarizes the μ^+ spin via the hyperfine (HF) interaction. Since the relaxation rate of electron spin is proportional to the excess carrier density Δn, the muon spin relaxation rate λ is sensitive to Δn, and can be used to measure its dynamics. However, this assumption is true only in the low rate regime (i.e., the relaxation rate of electron spin <HF frequency), and the microscopic exchange mechanism is discussed later in this Letter.

Our experiment has been carried out on a 500-μm thick intrinsic single crystal Si wafer (n-type, $R > 1000\ \Omega \cdot$ cm, both sides polished) with $\langle 111 \rangle$ axis perpendicular to the surface. As shown in Fig. 1(a), one side is facing the incoming pump light, whereas the other side faces the muon beam. Magnetic fields are applied either parallel (longitudinal field, LF) or perpendicular (transverse field, TF) to the direction of muon spin. Details of the experimental setup are explained elsewhere [7]. The distribution of stopped muon is centered in the wafer by adjusting the number of aluminum foil degraders, with its FWHM estimated to be $\approx$130 μm by a Monte Carlo simulation. Monochromatic 1064-nm laser light injects excess carriers almost uniformly throughout the sample by virtue of its low absorption in Si. Δn has been calculated based on an absorption coefficient $\alpha(293\ \mathrm{K}) = 14.32$ cm^{-1} measured in RT, and $\alpha(77\ \mathrm{K}) = 2.37 \times 10^{-2}$ cm^{-1} taken from the literature [19]. Because of the long absorption lengths compared with the wafer thickness, we assume that the central density represents Δn for the entire sample. The illuminated area on the sample is 9.6 cm^2, and it covers the entire area of the muon beam. With these geometries and the calculated carrier diffusion lengths ranging 100–200 μm, the surface effect is negligible in the obtained lifetime spectra. Figure 1(b) illustrates the pulse timing, in which muon pulses arrive at the sample at ΔT after laser pulses. Since the repetition rate of the laser and muon are 25 and (pseudo-)50 Hz respectively [7], the muon data are sorted and binned to "light ON" and "light OFF" spectra, and averaged for statistics, assuming that the photoinduced change is already over after 20 ms. In the optical setup, two attenuator assemblies and calibrated neutral density filters are used to accurately control the photon fluence for a wide range of carrier injection.

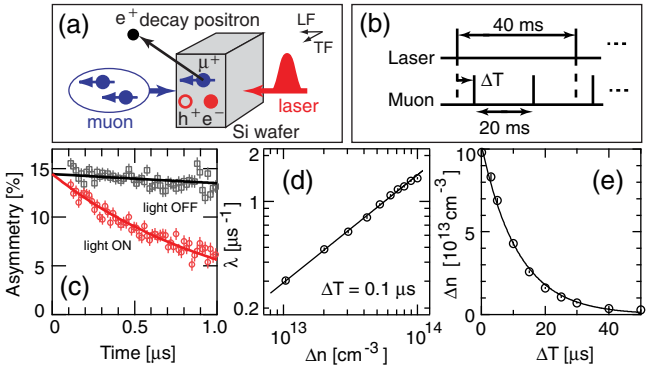

FIG. 1. (a) Schematic diagram of the experimental geometry. (b) Timing diagram of laser and muon pulse. Pulse duration (FWHM) of the laser and muon pulse are $\approx$16 and $\approx$70 ns respectively. (c) μSR time spectra for light OFF (black squares) and ON (red circles, $\Delta n = 4.7 \times 10^{13}$ cm^{-3}). 5×10^6 events are averaged for each spectrum. Fit parameters are $A(0) = 14.44(3)\%$, $\lambda' = 0.068(2)\ \mu\mathrm{s}^{-1}$ for light OFF, and $\lambda = 0.94(2)\ \mu\mathrm{s}^{-1}$ for light ON. (d) λ as a function of Δn. The fit (see text) gives $(\alpha, \beta\ [\mu\mathrm{s}^{-1}], \Delta n_0\ [\mathrm{cm}^{-3}]) = [0.68(4), 1.46(4), 8.9 \times 10^{13}]$. (e) Carrier decay curve. The fit (see text) gives $\Delta n(0) = 9.4(4) \times 10^{13}$ cm^{-3} and $\tau = 11.1(9)\ \mu$s.

Figure 1(c) shows representative light ON and OFF μSR time spectra in 291 K under LF 10 mT. The initially formed Mu_T^0 makes a rapid transition to Mu_{BC}^0, which is then quickly ionized to Mu_{BC}^+. Thus the light OFF spectrum is constituted of the diamagnetic Mu_{BC}^+ center, which shows a very small relaxation because the Zeeman interaction "locks" them along the field direction. Upon illumination at $\Delta T = 0.1$ μs, the muon spin asymmetry shows a significant relaxation. Based on the time scale of excess carrier recombination and the microscopic mechanism as described below, we use the first 1 μs in the spectrum as the fitting range assuming that Δn is constant in this period. The light OFF spectrum is fitted to $A(t) = A(0)e^{-\lambda' t}$ with $A(0)$ and λ' as fit parameters. The light ON spectrum is fitted in the same way but with fixed $A(0)$. This relaxation rate λ should be specific for the Δn because it arises as a consequence of the Mu-photocarrier interaction. We thus measure λ as a function of Δn [Fig. 1(d)], which can be fitted to a power law, $\lambda = \beta(\Delta n/\Delta n_0)^\alpha$, with α and β as fit parameters. From the obtained function, it is now possible to calculate Δn from a measured λ. As shown in Fig. 1(e), Δn is measured as a function of ΔT, where the carrier decay can be fitted to $\Delta n(\Delta T) = \Delta n(0)\exp[-\Delta T/\tau]$. Based on the obtained carrier lifetime, which is equivalent to τ_{SRH}, and an assumption that the defect type is interstitial iron, a common contaminant in Si, the SRH model estimates $N_t \approx 7 \times 10^{13}$ cm^{-3} for this wafer [20].

This lifetime spectroscopy using muons enables us to investigate τ_{bulk} in a wide range of injection level, an essential parameter for the IDLS measurement, by changing the magnitude of LF. For example, in LF 10 mT, the fit quality for light ON spectra becomes gradually worse when Δn exceeds 1×10^{14} cm^{-3} because the relaxation rate is too fast [see Fig. 1 (d)]. On the other hand if Δn is less than 1×10^{13} cm^{-3}, the fit quality is also poor because the relaxation is now too slow. It is however possible to change the "sensitivity" of Mu-carrier interaction by changing the magnitude of LF—this is corresponding to varying the Zeeman interaction of muon spin with respect to the Mu HF interaction [21]. In other words, a high field decouples the Mu HF interaction so that the μ^+ spin is less sensitive to the Mu-photocarrier interaction. Therefore, we can tune λ for the best fit quality depending on the injection levels. As shown in Fig. 2, three more injection levels have been measured for the λ *vs*. Δn curve. The decay curve for each field is measured in the same way as Fig. 1(e), and gives $\tau = 9.4(3)$, 9(1), and 9.2(8) μs for 0.2 T, 0.5 T, and 1.0 T, respectively. The SRH model with the calculated N_t predicts that τ_{SRH} is the fastest process and dominates τ_{bulk} up to $\Delta n \sim 10^{17}$ cm^{-3}, which agrees with the obtained lifetimes.

We now apply the method in a low temperature, 77 K, to demonstrate its feasibility for the temperature dependent measurements. Thermally activated transitions from the predominant Mu centers, Mu_T^0 and Mu_{BC}^0, are negligibly small in this temperature. Under low LF, the μSR signal relaxes fast because of the mobile Mu_T^0 (see below). As we have seen in Fig. 1(c) and 1(d), λ' sets the minimum λ usable in the λ *vs*. Δn curve. Therefore, for 77 K data, the LF magnitude has been changed to 0.15 T so that λ' is small, while Δn is in the same injection level as Fig. 1(d). The obtained λ *vs*. Δn and carrier decay curve can be found in Ref. [20]. The same analysis method gives $\tau = 1.8(1)$ μs. This significantly shorter carrier lifetime is associated with an increase of the capture cross section of defect centers. Considering that the temperature is too high for the cascade capture process to be predominant [22], the most likely mechanism is the excitonic Auger recombination [23].

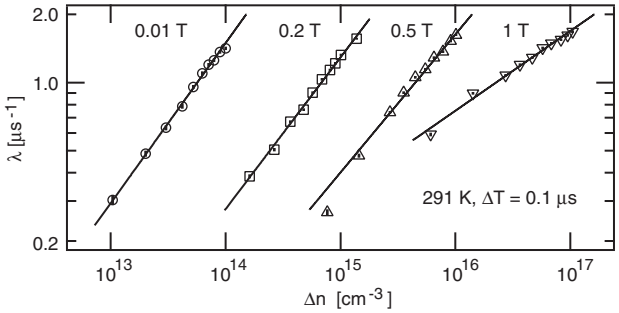

FIG. 2. λ is measured as a function of Δn under LF 10 mT [circles, identical to Fig. 1(d)], 0.2 T (squares), 0.5 T (triangles), and 1.0 T (inverted triangles). Solid lines denote the curve fits. Fit parameters for 0.2 T, 0.5 T, and 1.0 T are $(\alpha, \beta\ [\mu s^{-1}], \Delta n_0\ [cm^{-3}]) = [0.70(3), 1.33(3), 9.0 \times 10^{14}]$, $[0.61(6), 1.64(6), 8.6 \times 10^{15}]$, and $[0.34(3), 1.70(4), 9.9 \times 10^{16}]$, respectively.

The lifetime measurement in low temperature can also be performed using the precession signal of Mu_T^0, which is readily observable under a weak TF. The same procedure is applied to the Mu_T^0 signal under TF 0.2 mT to measure the λ *vs*. Δn curve, and subsequently the lifetime spectrum [20]. The difference here is that the Mu_T^0 precession in dark is already damped because of magnetic field inhomogeneity of the instrument and the quantum diffusion of Mu_T^0, which interacts with impurities in material [13]. Therefore the fit function for light ON should have a decay term, $e^{-(\lambda'+\lambda)t}$, to find the photoinduced rate separately. The obtained lifetime, $\tau = 1.3(3)$ μs, agrees well with the LF measurement, implying that both methods can observe the same excess carrier recombination. However the LF measurement is considered best suited for IDLS and TDLS applications because of the ability to tune the field for an interested injection level, and the applicability for a wide temperature range. The latter advantage is endorsed by previous photoexcited μSR studies on Si, which found a large photoinduced relaxation in the Mu_{BC} precession not only in the low temperature range continuously down to several Kelvins [17] but also in the high temperatures up to 550 K [18].

We have so far demonstrated the lifetime measurements based on the empirical observation that λ can be a useful

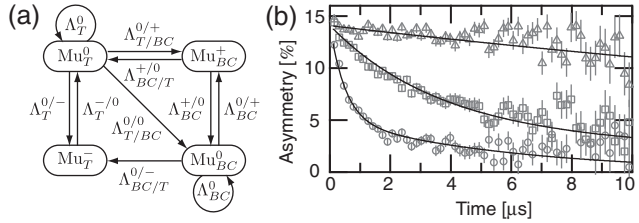

FIG. 3. (a) The four-state model of Mu in Si under illumination. The notation of Λ follows the convention in Ref. [17]. Its superscript and subscript indicate the charge-state and site change respectively with a slash between before and after the transition. Λ_T^0 and Λ_{BC}^0 indicate spin exchange interaction in Mu_T^0 and Mu_{BC}^0 with conduction electrons. (b) Representative light ON ($\Delta T = 0.1$ μs) μSR time spectra in 291 K under LF 10 mT for $\Delta n(0) = 1.0 \times 10^{14}$ cm^{-3} (circles), 1.6×10^{13} cm^{-3} (squares), and 1.4×10^{12} cm^{-3} (triangles). The solid lines denote the fit (see text).

yardstick of Δn. But what is the underlying microscopic mechanism? To answer this question it is necessary to study the model of Mu dynamics, which was originally used to analyze RF-μSR data [24], and later applied to a photoexcited μSR experiment [17]. The four-state model shown in Fig. 3(a) is based on the three-state model used by Fan *et al.*, but it has the Mu_T^- state in addition, which becomes more important for $\Delta n > 10^{14}$ cm^{-3} [17]. Transition from one Mu state to another is characterized by a transition rate Λ, which can depend on the capture cross section σ for electron/hole, electron/hole density, activation energy, and prefactor. Because this network is activated upon photocarrier injection, the μSR spectrum carries information for the dynamics of Mu transition, rather than a signal from static Mu states. To gain the comprehensive picture it is crucial to study a full μSR time spectrum, where Δn stays constant throughout. We therefore run the same set of experiments as Fig. 1 but using a thicker wafer with a longer carrier lifetime to satisfy this condition (see inset in Fig. 4). Figure 3(b) shows three representative μSR spectra out of eight Δn's. We perform a simultaneous fit for the spectra with σ's as global fit parameters, from which Λ's are

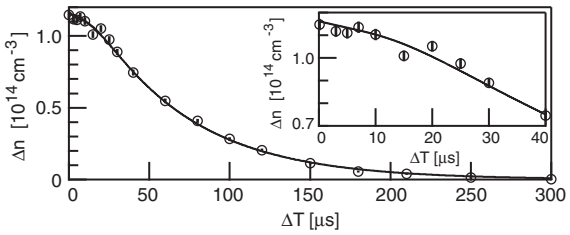

FIG. 4. Carrier decay curve for a 1000-μm thick intrinsic Si wafer (R > 10000 Ω · cm) in 291 K. Absorption coefficient α measured in RT = 6.80 cm^{-1}. Solid line denotes the fit (see text), which gives: $D = 12(2)$ cm^2/s, $\tau_{\text{bulk}} = 2(1) \times 10^2$ μs, and $\Delta n_c = 1.16(1) \times 10^{14}$ cm^{-3}. (*inset*) Magnified view shows the nearly constant Δn for $\Delta T < 10$ μs.

calculated based on the known Δn. This simulation and fit have been carried out using QUANTUM [25], a program to solve the time evolution of the muon spin using the density matrix method, running on MANTID [26]. See Ref. [20] for details of this computation. The fit result first tells us enhanced rates in $\Lambda_{BC}^{0/+}$ and $\Lambda_{BC}^{+/0}$ upon carrier injection. Because the rates are much faster than the HF frequencies in Mu_{BC}^0 (<92 MHz), the muon spin is hardly depolarized in this cycling transition. Second, a high Δn opens two channels, which "leaks" the Mu_{BC} states to the others. Some of Mu_{BC}^+ escape to the Mu_T^0 state via $\Lambda_{BC/T}^{+/0}$, where the HF interaction (2 GHz) depolarizes the muon spin—this is the fast relaxing part in Fig. 3(b). Others are converted from Mu_{BC}^0 to Mu_T^- via $\Lambda_{BC/T}^{0/-}$, which is an inert, less interactive Mu center with carriers—and this is the subsequent slow relaxing tail. As Δn decreases, these channels become narrower, resulting in isolated Mu_{BC}. Slow decay in the lowest Δn in Fig. 3(b) is thus attributed to Λ_{BC}^0 causing the relaxation during the fleeting window when the cycling Mu_{BC} state is in Mu_{BC}^0. Based on these observations, we conclude that the first 1 μs window used in the lifetime measurement corresponds to primarily fitting the fast Mu_T^0 relaxation. Tuning the Mu sensitivity in a higher field (Fig. 2) is equivalent to decoupling the HF interaction in Mu_T^0. The sublinear dependence of λ on Δn (i.e., $\alpha \approx 0.7$) stems from the transition path for Mu_{BC}^0 leading to Mu_T^-.

Finally, Fig. 4 shows the carrier decay curve for the long-lifetime wafer. The curve is apparently different from the single exponential decay, but it has a shoulder of around 20 μs, where the fast surface recombination driven by carrier diffusion comes into play. This lifetime spectrum can be modeled with a simple one-dimensional diffusion equation for $\Delta n(z,t)$, $D(\partial^2 \Delta n/\partial z^2) - (\Delta n/\tau_{\text{bulk}}) = (\partial \Delta n/\partial t)$, where D is the carrier diffusion constant. Because the wafer surfaces have been lapped and chemically polished, the surface velocity should be $>10^4$ cm/s. We therefore assume a boundary condition on the surfaces, $\Delta n(0,t) = \Delta n(d,t) = 0$, and analytically solve the equation with an initial condition, $\Delta n(z,0) = \Delta n_c$. With D, τ_{bulk}, and Δn_c as fit parameters, the solid line in Fig. 4 shows a fit to $\Delta n(d/2,t)$. The obtained $\tau_{\text{bulk}} = 2(1) \times 10^2$ μs agrees with $\tau_{\text{bulk}} \approx 1 \times 10^2$ μs, which has been measured by the wafer manufacturer (PI-KEM Ltd.) using the standard PCD method.

In conclusion, excess carrier lifetime in Si has been measured using photoexcited μSR. This novel technique enables us to measure τ_{bulk} directly by virtue of the implanted muons as a bulk probe, and can access a wider range of recombination lifetime (from 50 ns to >20 ms), injection level, and temperature. The four-state model can explain the underlying microscopic mechanism about how λ exhibits the dependence on Δn. The high time resolution is possible only with a short-pulsed laser, and it

distinguishes this study from the previous experiments using lamps. The precisely controlled Δn is achievable with the collimated beam and narrow linewidth, which gives a predictable uniform absorption profile in the sample. The method can be applied immediately to other semiconductors, such as Ge and GaAs, where the Mu-photocarrier interaction has already been reported [27,28]. Its capability on measuring recombination kinetics can be useful in emerging high-efficiency light harvesting materials.

This work has been supported by European Research Council (Proposal No 307593—MuSES). We wish to acknowledge the assistance of a number of technical and support staff in ISIS and Queen Mary Univ. of London.

*koji.yokoyama@stfc.ac.uk
†a.j.drew@qmul.ac.uk

[1] D. K. Schroder, *Semiconductor Material and Device Characterization*, 3rd ed. (John Wiley & Sons, Inc., Hoboken, 2006).
[2] S. Rein, *Lifetime Spectroscopy: A Method of Defect Characterization in Silicon for Photovoltaic Applications* (Springer Science & Business Media, Berlin, 2006).
[3] D. V. Lang, Deep-level transient spectroscopy: A new method to characterize traps in semiconductors, J. Appl. Phys. **45**, 3023 (1974).
[4] S. Rein, T. Rehrl, W. Warta, and S. W. Glunz, Lifetime spectroscopy for defect characterization: Systematic analysis of the possibilities and restrictions, J. Appl. Phys. **91**, 2059 (2002).
[5] S. Rein and S. W. Glunz, Electronic properties of the metastable defect in boron-doped Czochralski silicon: Unambiguous determination by advanced lifetime spectroscopy, Appl. Phys. Lett. **82**, 1054 (2003); Electronic properties of interstitial iron and iron-boron pairs determined by means of advanced lifetime spectroscopy, J. Appl. Phys. **98**, 113711 (2005).
[6] A. Cuevas and D. Macdonald, Measuring and interpreting the lifetime of silicon wafers, Sol. Energy **76**, 255 (2004).
[7] K. Yokoyama *et al.*, The new high field photoexcitation muon spectrometer at the ISIS pulsed neutron and muon source, Rev. Sci. Instrum. **87**, 125111 (2016).
[8] K. Yokoyama, P. Murahari, P. Heathcote, L. Nuccio, J. S. Lord, N. A. Morley, and A. J. Drew, Future directions of μSR—Laser excitation, Phys. Scr. **88**, 068511 (2013).
[9] K. Wang *et al.*, Temporal mapping of photochemical reactions and molecular excited states with carbon specificity, Nat. Mater. **16**, 467 (2017).
[10] J. S. Lord *et al.*, Design and commissioning of a high magnetic field muon spin relaxation spectrometer at the ISIS pulsed neutron and muon source, Rev. Sci. Instrum. **82**, 073904 (2011).
[11] S. J. Blundell, Spin-polarized muons in condensed matter physics, Contemp. Phys. **40**, 175 (1999).
[12] L. Nuccio, L. Schulz, and A. J. Drew, Muon spin spectroscopy: magnetism, soft matter and the bridge between the two, J. Phys. D **47**, 473001 (2014).
[13] B. D. Patterson, Muonium states in semiconductors, Rev. Mod. Phys. **60**, 69 (1988).
[14] S. F. J. Cox, Muonium as a model for interstitial hydrogen in the semiconducting and semimetallic elements, Rep. Prog. Phys. **72**, 116501 (2009).
[15] R. Kadono, A. Matsushita, R. M. Macrae, K. Nishiyama, and K. Nagamine, Muonium Centers in Crystalline Si and Ge under Illumination, Phys. Rev. Lett. **73**, 2724 (1994).
[16] R. Kadono, R. M. Macrae, and K. Nagamine, Charge dynamics of muonium centers in Si revealed by photo-induced muon spin relaxation, Phys. Rev. B **68**, 245204 (2003).
[17] I. Fan, K. H. Chow, B. Hitti, R. Scheuermann, W. A. MacFarlane, A. I. Mansour, B. E. Schultz, M. Egilmez, J. Jung, and R. L. Lichti, Optically induced dynamics of muonium centers in Si studied via their precession signatures, Phys. Rev. B **77**, 035203 (2008).
[18] K. H. Chow, I. Fan, M. Egilmez, J. Jung, and B. Hitti, μSR and photo-excitation of Si above room temperature, Phys. Procedia **30**, 210 (2012).
[19] G. G. Macfarlane, T. P. McLean, J. E. Quarrington, and V. Roberts, Fine structure in the absorption-edge spectrum of Si, Phys. Rev. **111**, 1245 (1958).
[20] See Supplemental Material at http://link.aps.org/supplemental/10.1103/PhysRevLett.119.226601 for calculation of defect density using the SRH model, carrier lifetime measurements in low temperature, and details about computation of the four-state model.
[21] K. H. Chow, B. Hitti, and R. F. Kiefl, in *Semiconductors and Semimetals*, edited by M. Stavola (Elsevier, New York, 1998), pp. 137–207.
[22] M. Lax, Cascade capture of electrons in solids, Phys. Rev. **119**, 1502 (1960).
[23] A. Hangleiter, Nonradiative recombination via deep impurity levels in semiconductors: The excitonic Auger mechanism, Phys. Rev. B **37**, 2594 (1988).
[24] S. R. Kreitzman, B. Hitti, R. L. Lichti, T. L. Estle, and K. H. Chow, Muon-spin-resonance study of muonium dynamics in Si and its relevance to hydrogen, Phys. Rev. B **51**, 13117 (1995).
[25] J. S. Lord, Computer simulation of muon spin evolution, Physica (Amsterdam) **374–375B**, 472 (2006).
[26] O. Arnold *et al.*, Mantid—Data analysis and visualization package for neutron scattering and μSR experiments, Nucl. Instrum. Methods Phys. Res., Sect. A, **764**, 156 (2014).
[27] I. Fan, K. H. Chow, B. Hitti, R. Scheuermann, A. I. Mansour, W. A. MacFarlane, B. E. Schultz, M. Egilmez, J. Jung, Y. G. Celebi, H. N. Salameh, B. R. Carroll, J. E. Vernon, and R. L. Lichti, Influence of photoexcitation on the diamagnetic muonium states in Ge studied via their precession signatures, Phys. Rev. B **78**, 153203 (2008).
[28] K. Yokoyama *et al.*, Detection of conduction electron spin polarization in n-GaAs by negative muonium, Phys. Procedia **30**, 231 (2012).